Investigation and optimization of parameters affecting the multiply charged ion yield in AP-MALDI MS

Article

Published Version

It is advisable to refer to the publisher's version if you intend to cite from the work.

www.reading.ac.uk/centaur

CentAUR

Central Archive at the University of Reading

Reading's research outputs online

CrossMark

Investigation and optimization of parameters affecting the multiply charged ion yield in AP-MALDI MS

Pavel Ryumin [a], Jeffery Brown [a,b], Michael Morris [b], Rainer Cramer [a,*]

[a] Department of Chemistry, University of Reading, Whiteknights, Reading RG6 6AD, UK
[b] Waters Corporation, Stamford Avenue, Wilmslow SK9 4AX, UK

A B S T R A C T

Liquid matrix-assisted laser desorption/ionization (MALDI) allows the generation of predominantly multiply charged ions in atmospheric pressure (AP) MALDI ion sources for mass spectrometry (MS) analysis. The charge state distribution of the generated ions and the efficiency of the ion source in generating such ions crucially depend on the desolvation regime of the MALDI plume after desorption in the AP-to-vacuum inlet. Both high temperature and a flow regime with increased residence time of the desorbed plume in the desolvation region promote the generation of multiply charged ions. Without such measures the application of an electric ion extraction field significantly increases the ion signal intensity of singly charged species while the detection of multiply charged species is less dependent on the extraction field. In general, optimization of high temperature application facilitates the predominant formation and detection of multiply charged compared to singly charged ion species. In this study an experimental set-up and optimization strategy is described for liquid AP-MALDI MS which improves the ionization efficiency of selected ion species up to 14 times. In combination with ion mobility separation, the method allows the detection of multiply charged peptide and protein ions for analyte solution concentrations as low as 2 fmol/μL (0.5 μL, i.e. 1 fmol, deposited on the target) with very low sample consumption in the low nL-range.

© 2016 The Authors. Published by Elsevier Inc. This is an open access article under the CC BY license (http://creativecommons.org/licenses/by/4.0/).

1. Introduction

Matrix-assisted laser desorption/ionization (MALDI) [1,2] and electrospray ionization (ESI) [3] are key ionization techniques for the analysis of biomolecules by mass spectrometry (MS). The pulsed nature of MALDI makes it more amenable to coupling with axial time-of-flight (TOF) mass analyzers with the ionization event occurring in a high-vacuum region. On the other hand, ESI was developed at atmospheric pressure (AP) and like many other AP sources is coupled to mass analyzers designed for analysis of continuous ion beams, including tandem quadrupole and orthogonal TOF-based systems [3–5]. Although ion generation at ambient pressure requires efficient ion transportation to the high-vacuum regions of the mass analyzer, the ion source operation at elevated pressures provides more facile coupling of powerful analytical separation techniques such as liquid chromatography, and within the mass spectrometer, gas-phase techniques such as tandem mass spectrometry (MS/MS) [6] and ion mobility [7] separation. In the last few years, there has been an ongoing effort to adapt these

developments for MALDI [8–14]. In 2000, Laiko et al. [15] reported an ion source with a common instrumental platform incorporating both ESI and AP-MALDI ion sources [15–17]. Recently it was discovered that, under certain conditions, AP-MALDI ion sources generate predominantly multiply charged ions [18–20], with similar abundances to those typically generated by ESI.

Multiply charged ions are often more suitable for MS analysis than singly charged. For instance, for microchannel plate (MCP) detectors, which are typically used in TOF MS, the ion-electron yield depends on the impact velocity and energy of the primary ion beam, which in turn depends on the charge and mass value of the ion [21], typically leading to the discrimination against ions with low charges and/or higher m/z values. In Fourier transform (FT)-based mass analyzers, such as Orbitraps and FT-ICR instruments, the measured analyte ion oscillation frequency depends on the m/z ratio [22,23], resulting in higher resolving power for the same acquisition time if the m/z value is lower. Furthermore, many commercial mass spectrometers include radio frequency (RF) ion guides or ion manipulation devices that have a limited m/z transmission range [24].

Another major advantage of multiply charged ions can be found in their superior fragmentation spectra. According to a number of

publications [25–27], collision-induced dissociation (CID) fragmentation spectra of doubly charged peptide precursor ions provide different and often enhanced information compared to the spectra obtained by fragmentation of singly charged ions. The recently developed electron-capture dissociation (ECD) [28] and electron-transfer dissociation (ETD) [29] fragmentation methods preserve labile post-translational modifications and therefore provide complementary information to CID. The core of the ECD and ETD fragmentation process involves the capture of an electron by the precursor cation, reducing its charge state. It is therefore a requirement that the precursor ion is at least doubly charged in order to have product ions for detection.

In conventional MALDI, ions are typically singly charged and the process of ion generation is still not fully understood. However, two theories persist: the first is the gas phase protonation model [30–33] and the second is known as the 'Lucky Survivor' model [34,35]. The 'Lucky Survivor' model is based on the premise that analyte ions are preformed before ablation, while the gas phase protonation model suggests that neutral analyte molecules are protonated after ablation. Both models agree that gas phase chemistry and particularly the recombination processes with the oppositely charged species during rapid plume expansion play an important role in the ionization process and account for the observed predominantly singly charged ion yield [34,36]. Frankevich et al. have shown that in conventional MALDI experiments the charge state distribution of the generated analyte ion yield can be shifted to higher charge states by using a dielectric MALDI target plate and low laser fluence [37]. They attributed this shift to a decrease in the ion recombination rate due to a lower number of 'free electrons' in the MALDI plume. However, the proportion of the detected multiply protonated analytes remained inferior to the proportion of the detected singly protonated analytes [37].

Owing to the similarity of the generated predominantly multiply charged ions in the recently developed laserspray and liquid AP-MALDI approaches to ESI [19,20], it has been hypothesized that the ion formation is based on similar mechanisms. In ESI initially highly charged liquid droplets containing analyte molecules are dispersed into the gas phase. These droplets evaporate and undergo Coulomb fission upon reaching the Rayleigh limit. Two main mechanisms were proposed for the next step of gas phase ion generation, namely the charge residue model (CRM) [38] and the ion evaporation model (IEM) [39,40]. In the CRM solvent droplet fission leads to a charged progeny droplet with one analyte molecule and the ion is released when all the solvent evaporates. In the IEM, when the droplet reaches a certain radius, the applied electric field becomes sufficient to field-desorb charged analytes. Both models predict the ion release on later stages of the droplets evolution with sufficient desolvation being a prerequisite [41].

A major limitation of all AP ion sources with respect to performance is the loss of ions associated with their transfer into the analyzer's vacuum regions. Extensive research has been carried out to design more efficient interfaces with a particular emphasis on supplying additional energy to the transferred ion plume for both ESI [42–44] and AP-MALDI [15,45–47]. This can play a major role in the desolvation and declustering during the ionization process in ESI [41] and also help in declustering the generated MALDI plume [35]. Another important consideration for the design of an AP interface is the transmission of ions in the ion transfer tube (or capillary) which may be affected by the gas flow regime, transit time and temperature in the transfer region [48–51]. In this work the influence of desolvation conditions in the ion source and ion transfer region on the detected ion signal from the liquid AP-MALDI ion source is discussed. A new interface design, which allows the optimization of both the flow regime and temperature in the heated ion transfer tube is described, and the transmission biases with respect to the detected charge state similar to what has been previously reported for ESI [52,53] are discussed.

2. Materials and methods

2.1. MALDI sample preparation

A two-peptide mixture containing [Val]^5-angiotensin I (Sigma-Aldrich, Poole, UK) and bradykinin (Sigma-Aldrich) was prepared in water containing 0.1% formic acid (Greyhound, Birkenhead, UK) at concentrations of 50 pmol/μL for the experiments at ambient temperatures, i.e. without external heating, and 10 pmol/μL for the experiments with external heating. In addition, a [Val]^5-angiotensin I solution was prepared at a concentration of 2 fmol/μL in water containing 0.1% formic acid for assessing the limit of detection (LOD). Two matrix solutions were prepared using the
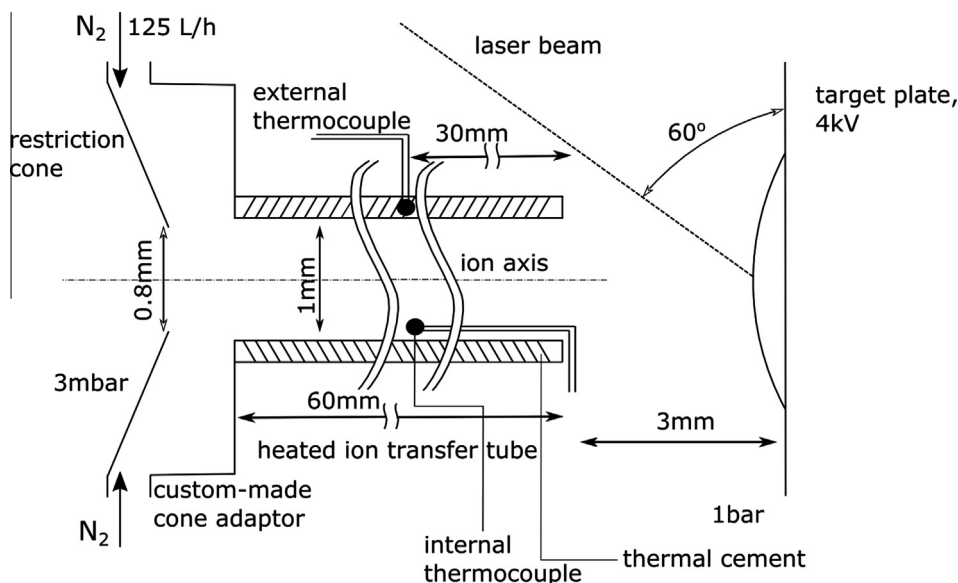

Fig. 1. Schematic of the AP-MALDI ion source and modified AP-to-vacuum interface used for the production of multiply protonated molecules. The experimental values given represent the optimum values for the detection of multiply protonated peptides in liquid AP-MALDI MS experiments.
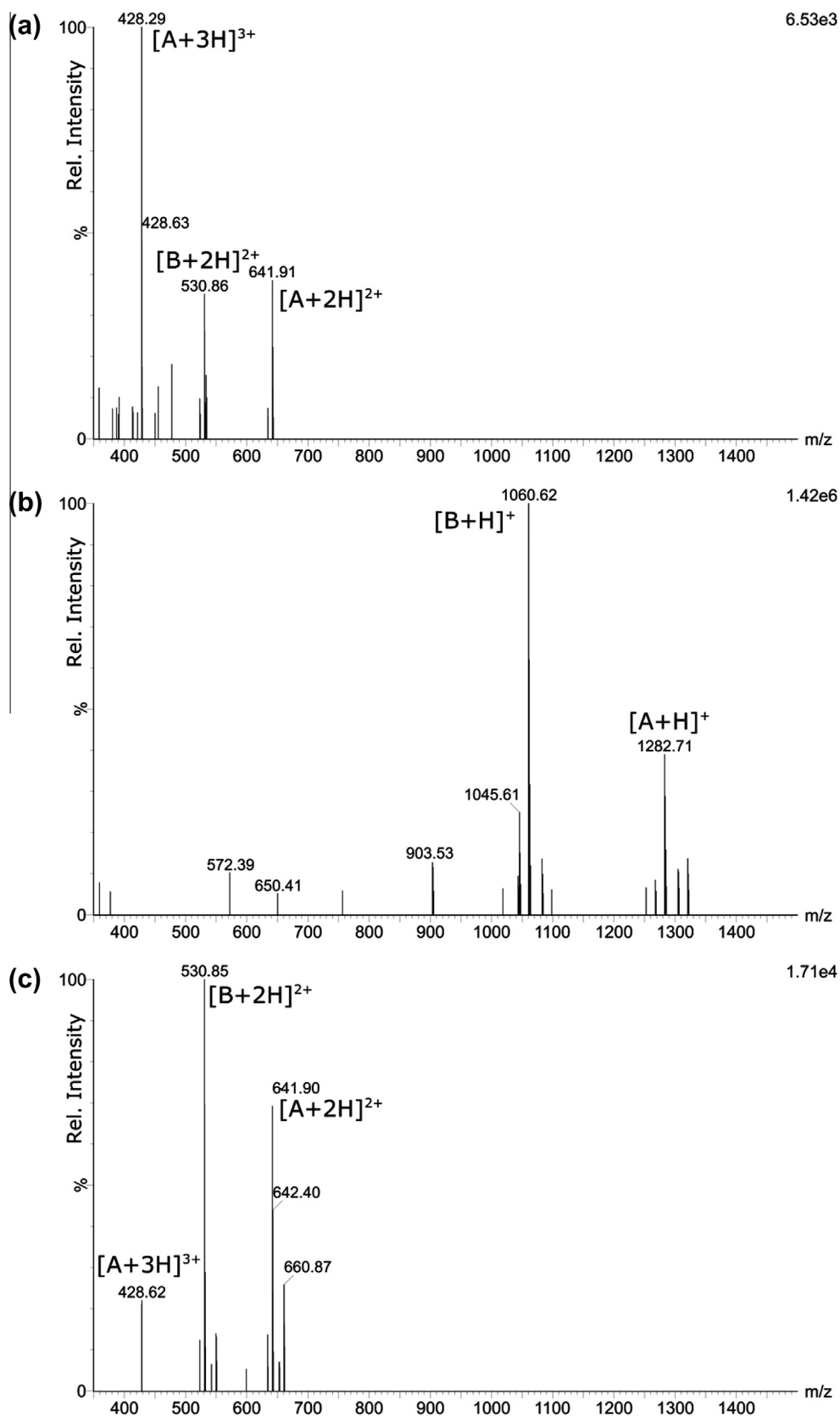
Fig. 2. Liquid AP-MALDI mass spectra of 25 pmol each of [Val5]-angiotensin I and bradykinin on the target plate acquired without heating the ion transfer tube. a) Spectrum acquired under favourable conditions for the detection of multiply protonated analytes: the target plate was placed 9 mm away from the entrance of the ion transfer tube and the extraction potential difference was set to 0 V. b) Spectrum acquired under favourable conditions for the detection of singly protonated analytes: the target plate was placed 3 mm away from the entrance of the ion transfer tube and the extraction potential difference was set to 4 kV. c) Spectrum obtained by filtering out ion signals of singly charged species from the data shown in b) using the information obtained by ion mobility. In all spectra A and B denote [Val5]-angiotensin I and bradykinin, respectively. The base peak intensity is shown in the top right corner for each spectrum.
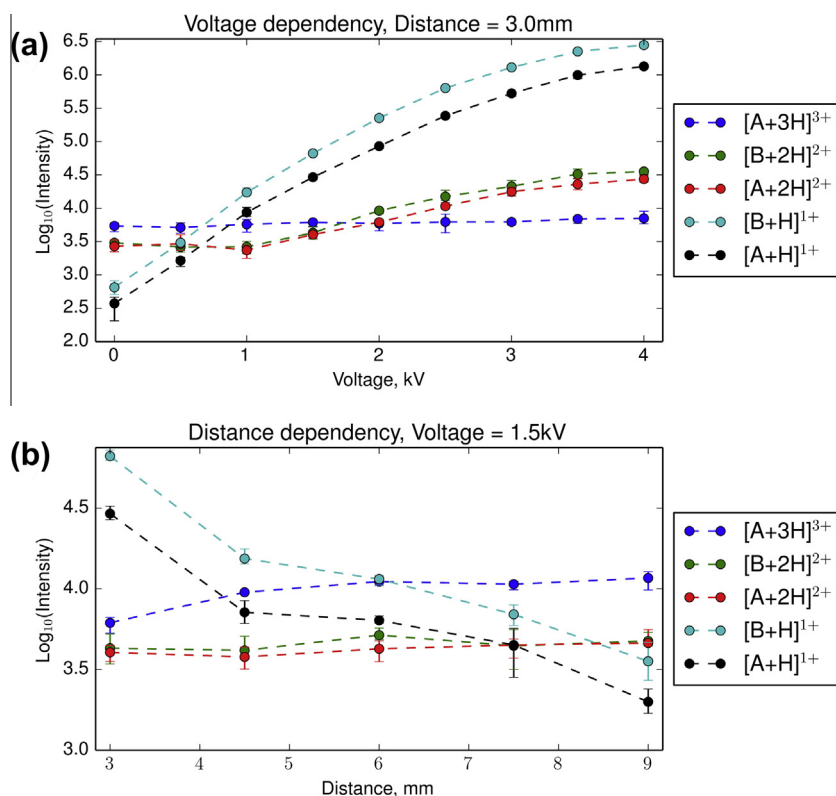
Fig. 3. (a) Voltage dependency of the absolute intensity of the protonated bradykinin (B) and [Val[5]]-angiotensin I (A) ion species with various charge states acquired without any heating of the ion transfer tube. The target plate was placed 3 mm away from the entrance of the ion transfer tube. (b) Distance dependency of the absolute intensity of the protonated bradykinin and [Val[5]]-angiotensin I ion species with various charge states acquired without any heating of the ion transfer tube. The extraction potential difference was set to 1.5 kV. For both plots A and B denote [Val[5]]-angiotensin I and bradykinin, respectively. All measurements were performed in triplicates. Error bars reflect the data distribution.

same protocol with 2,5-dihydroxybenzoic acid (DHB; Sigma-Aldrich) being dissolved in 70% acetonitrile at the concentration of 25 mg/mL for the LOD experiment and 100 mg/mL for all other experiments. Each solution was put into an ultrasonic bath for 15 min, and to each 60% of glycerol (Sigma-Aldrich) was added by volume. A pipette tip was used to disrupt the interface between the DHB solution and the glycerol layer in each preparation. Subsequently, the matrix solutions were put again into an ultrasonic bath for 15 min. Finally, an aliquot of 0.5 μL of the analyte solution was spotted with 0.5 μL of the matrix solution and mixed on the MALDI target plate. The spotted droplets were left for 5 min under ambient conditions before MS data acquisition and remained liquid during the entire analysis.

2.2. AP-MALDI ion source set-up

A commercial Synapt G2-Si mass spectrometer (Waters Corporation, Wilmslow, United Kingdom) equipped with an AP nano-LockSpray ESI ion source was modified (see Fig. 1). The source housing was machined to allow laser beam access, and an additional mounting plate was attached to the instrument housing to provide a platform for a MALDI target plate positioning assembly. This assembly consists of an XY translational stage for the sample positioning and a Z translational stage for adjusting the distance to ~3 mm between the target plate and the inlet of a custom-built ion transfer tube that is attached to the normal mass spectrometer inlet. The target plate holder is electrically isolated from the stage assembly by PEEK spacers, and a high voltage potential provided by the instrument's ESI ion source power supply is connected to the stainless steel target plate. Where needed, interlocks are overridden to enable the operation of the mass spectrometer with the custom-made source. (Please note that local H&S requirements, *e.g.* regarding laser safety and risk assessments, have to be satisfied as it was the case for this study.) An optical breadboard is mounted on top of the instrument to accommodate a 337 nm nitrogen laser (MNL 103 LD; LTB Lasertechnik GmbH, Berlin, Germany), typically operating at 10 Hz with a maximum pulse energy of 100 μJ and pulse width of 3 ns. A neutral density filter is used to moderate the laser pulse energy. The laser beam is guided by mirrors to the target plate in reflection geometry. Final focusing and steering of the laser beam is done by a lens with 150 mm focal length and a mirror located between the lens and the target plate. The position of the mirror provides the smallest practically possible laser beam incidence angle on the target of approximately 30°. As the alignment of the laser desorption spot with the ion transfer tube axis is important, the described system was designed to preserve this alignment during spot size adjustment. High shot-to-shot reproducibility of the MS ion signal intensity from the liquid MALDI samples allows accurate optimization of the laser spot size and X-Y position.

2.3. AP-to-vacuum interface

For the AP-to-vacuum interface, the standard sample cone assembly attached to the ion block of the commercial ESI ion source is replaced with a custom-made cone adaptor, to which a 60 mm-long interchangeable ion transfer tube with an inner diameter of 1 mm is attached (see Fig. 1). To promote cluster desolvation the ion transfer tube is resistively heated with a NiCr wire, which is powered by a low-voltage DC power supply (0–5 A, 0–30 V) and has a resistance of ~6 Ω. The wire is electrically insulated from the ion transfer tube by a layer of high temperature
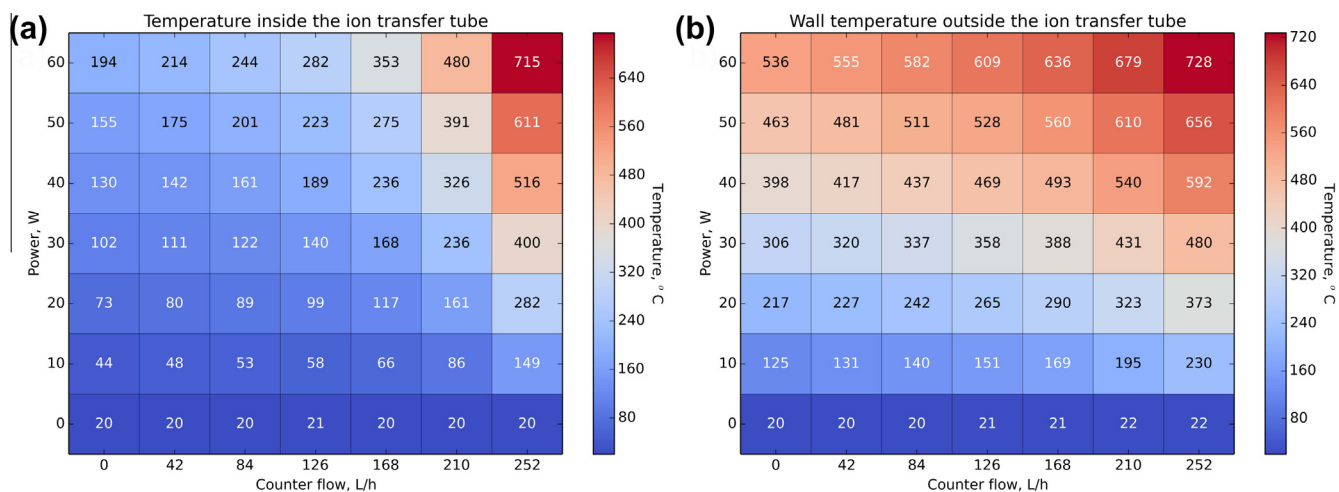
Fig. 4. (a) Relationship between the gas temperature inside the heated ion transfer tube and the applied heating power and counter flow. The temperature was measured by a K-type thermocouple without isolation inserted 30 mm into the ion transfer tube. (b) Relationship between the outer wall temperature of the ion transfer tube and the applied heating power and counter flow. Temperature was measured in the middle of the heated region with a K-type thermocouple being embedded into the thermal paste insulation. For both plots a higher counter flow value corresponds to a lower gas flow value in the ion transfer tube towards the entry of the mass analyzer. Stationary flow conditions are achieved at a counter flow value of approximately 265 L/h.

cement (OMEGABOND® 600 Powder; Omega Engineering Ltd, Manchester, UK) and evenly wound over its entire length. A second layer of high temperature cement is used to fix the wire and to embed a K-type thermocouple with a diameter of 0.25 mm (5SRTC-GG-KI-30-1M; Omega Engineering Ltd). This thermocouple is used to monitor the wall temperature of the ion transfer tube. For the temperature measurements inside the ion transfer tube a second K-type thermocouple (5SRTC-GG-KI-30-1M) was inserted 30 mm deep inside the heated region of the tube. In order to minimize the footprint of the thermocouple placed inside the ion transfer tube its electrical insulation layer was removed, reducing its influence on the gas flow. The above set-up did not allow determination of the exact position where the temperature was measured in the ion transfer tube but provided a mean temperature of the gas flow around the thermocouple.

The cone adapter holds the inner cone with a 0.8 mm orifice, which separates the heated ion transfer region from the first pumping stage. The standard ion block is further equipped with a port for nitrogen gas ('Cone Gas') which is introduced at ambient temperature with a controllable gas flow to stabilize the ESI spray plume. In this arrangement, the gas is directed into the exit region of the ion transfer tube and effectively reduces the plume/gas flow within and towards the entry of the ion transfer tube. A schematic of the interface modifications as well as the optimum experimental conditions for the detection of multiply protonated peptides in liquid AP-MALDI MS experiments using this modified Synapt G2-Si mass spectrometer are shown in Fig. 1.

2.4. MS data acquisition

All data were acquired in ESI mode with all API gases apart from the 'Cone Gas' being turned off. The 'Sampling Cone' and 'Source Offset' parameter values were set to 40 V and 80 V, respectively. For ion mobility experiments, the drift time in the ion mobility separation cell was recorded using default parameter settings (IMS Wave Velocity: 650 m/s; IMS Wave Height: 40.0 V). The ion block temperature in all experiments was set to 80 °C unless otherwise mentioned. The m/z range for all data acquisitions was set to 100–2000. Measurements were partially automated using Waters Research Enabled Software (WREnS). This software was used to run a script, which sets certain instrumental parameters for specific acquisition scans. Ion signal intensities and their dependencies

on parameters such as target plate potential and counter flow were investigated. Unless mentioned otherwise data points acquired for such dependencies were averaged over 30 scans with the scan duration set to 1 s. One sample spot was used to acquire automatically 7 and 9 data points for the dependency of the ion signal intensity on counter gas flow and target plate potential, respectively.

2.5. MS data processing

All data files were converted to the mzML data format using the msconvert utility from the ProteoWizard software package (version 3.0.6893) [54]. In-house developed software based on the Batmass software package (version 0.0.4) [55] was used to automatically extract the integrated ion intensities of interest from the converted data files. Prior to the extraction of multiply charged ion signals, singly charged ion signals were filtered out using the software Driftscope (version 2.6; Waters). All spectra were centroided with the automatic peak detection option of the MassLynx software (version 4.1; Waters).

3. Results and discussion

3.1. Generation of multiply protonated molecules without heating the ion transfer tube

Given that the standard commercial AP-ESI ionization interface sufficiently desolvates and declusters electrospray plumes, initial testing was undertaken for the detection of multiply charged analytes using a liquid AP-MALDI target assembly without the ion transfer tube attached to the modified cone assembly. In these experiments it was observed that changing the ion block temperature setting from the minimum of 30 °C to the maximum of 150 °C did not significantly change the detected analyte ion signal, which predominantly consisted of singly protonated species. This and the observed high LOD in the low picomole range were in contrast to previously reported results [20], where the detected analyte ion signal predominantly represented multiply charged species and was strongly dependent on the desolvation temperature. This suggests that the desolvation capabilities of the unmodified commercial AP-ESI ionization interface were insufficient for liquid
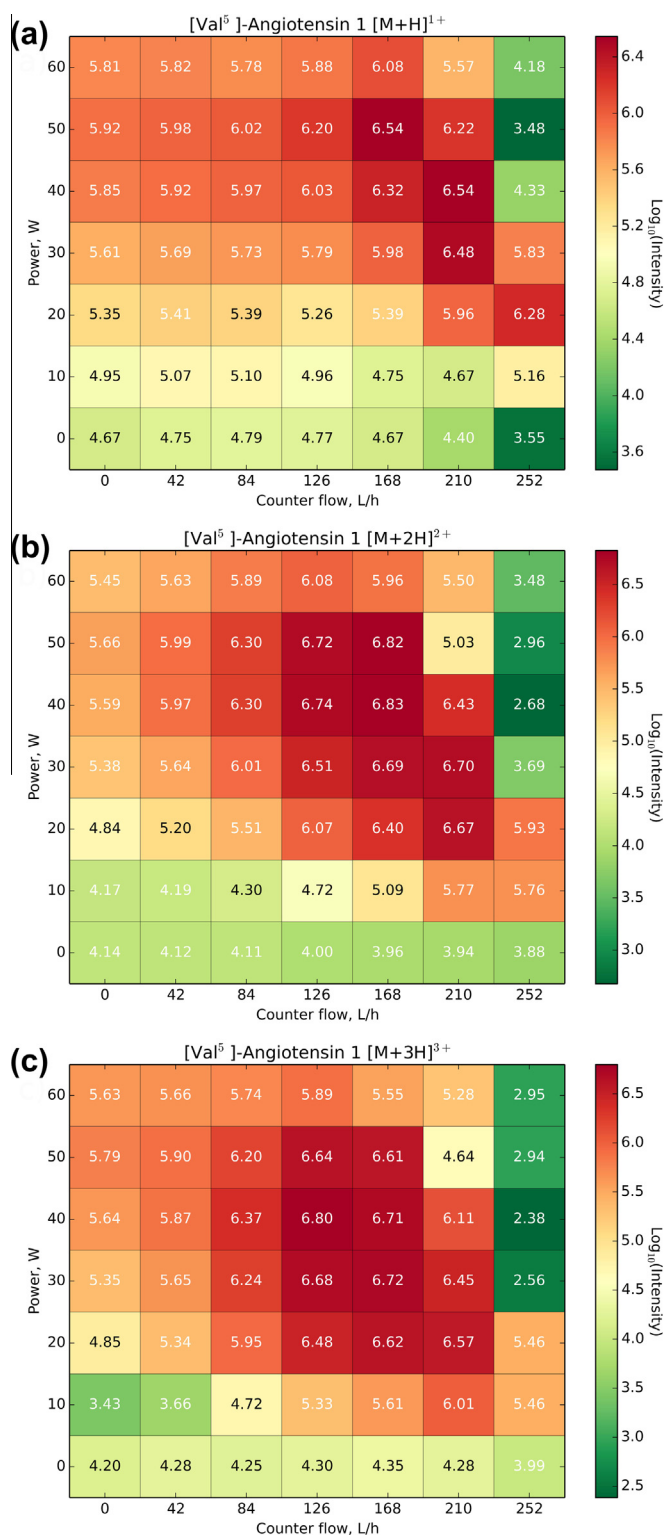
Fig. 5. Liquid AP-MALDI MS signal intensities of protonated [Val^5]-angiotensin I ion species acquired under different desolvation conditions. The data was acquired using a 0.8 mm restriction cone orifice and a 60 mm-long heated ion transfer tube with a 1 mm inner diameter. The extraction potential difference was set to 3 kV and the target plate was placed 3 mm away from the entrance of the ion transfer tube. a), b) and c) represent extracted ion signal intensities for singly, doubly and triply protonated [Val^5]-angiotensin I.

AP-MALDI. Interestingly, in further experiments with the ion transfer tube attached it was found that the charge state of the most abundant analyte ion signals depends on the potential applied to

the target plate as well as the distance between the ion transfer tube and target plate.

To study this phenomenon further, a set of experiments was carried out under the same experimental conditions, varying only the applied target potential and the distance between the ion transfer tube and target plate. For these experiments, the ion transfer tube heating was turned off and the ion block temperature was set to 30 °C to ensure that no additional heat is provided during the travel of the MALDI plume to the inlet of the mass analyzer. An amount of 25 pmol of [Val^5]-angiotensin I and bradykinin each was spotted on the target. The laser energy was set to its maximum of 100 µJ and the laser beam was focused on the target to a spot size diameter of approximately 200–300 µm in order to obtain the highest signal intensity.

In Fig. 2 mass spectra are shown that were acquired under optimal conditions for the detection of multiply protonated analytes (Fig. 2a; no extraction field and a distance of 9 mm between the ion transfer tube and target plate) and for the detection of singly protonated analytes (Fig. 2b; extraction potential difference of 4 kV and a distance of 3 mm between the ion transfer tube and target plate) without the application of post-acquisition ion filtering using the information obtained by ion mobility. Interestingly, the multiply protonated analyte signal intensities of the former are two orders of magnitude lower than the singly protonated analyte signal intensities of the latter. However, if elimination of singly charged ion signal by ion mobility filtering is applied to the latter (Fig. 2c), it can be seen that the absolute signal intensities of multiply protonated analytes are similar to the intensities that were obtained under optimal conditions without ion mobility filtering (Fig. 2a) albeit with a noticeable intensity shift from the triply protonated to the doubly protonated species. As all spectra were acquired under the same conditions apart from the extraction potential and distance between the ion transfer tube and target plate, these data suggest that there are different parameters and processes involved in the generation of singly protonated compared to multiply protonated analytes. Similar results were previously reported for laserspray ionization [56], suggesting that both share essential steps of the ionization process as well as a clear difference between the ion formation of MALDI-like singly protonated and ESI-like multiply protonated species.

Other data revealed that the ion signal of singly protonated peptides increases by up to four orders of magnitude with an increasing extraction field while only a slight or no increase was obtained for multiply protonated analytes. For instance, for a distance of 3 mm between the ion transfer tube and target plate, the signal intensities of both singly protonated bradykinin and singly protonated [Val^5]-angiotensin I substantially increased with the extraction potential/field, while the intensities of the doubly protonated species only slightly increased and virtually not at all for the triply protonated [Val^5]-angiotensin I (Fig. 3a). These data support the hypothesis that the ion formation of the different charge states proceeds via different mechanisms and possibly occurs in different places. In particular, it supports the hypothesis that singly protonated molecules are formed by conventional MALDI mechanisms at the very early stages of the MALDI plume close to the target and therefore well within the ion extraction field. In this case higher extraction fields could prevent ion recombination and improve the efficient collection of the generated molecular ions towards the mass spectrometer inlet. Multiply protonated species on the other hand could be predominantly generated from the ablated charged droplets via ESI-like mechanisms with the analyte ion liberation occurring later in the (field-free) region of the ion transfer tube.

Additional data obtained from changing the extraction field by changing the distance between the ion transfer tube and target plate at constant extraction potential further substantiate the
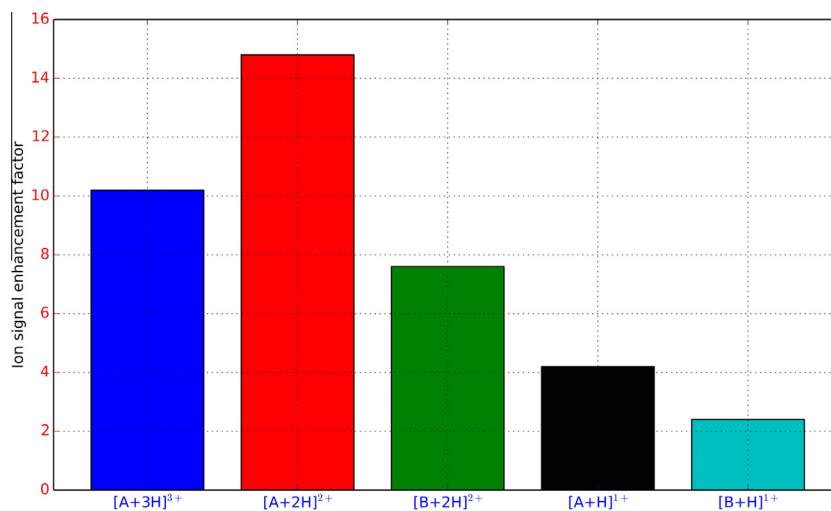
Fig. 6. Analyte ion signal enhancements in liquid AP-MALDI MS achieved by optimizing two parameters, the counter gas flow and heating power, compared to just one parameter, the heating power. The same raw data used for Fig. 5 (including data for bradykinin) were further analyzed by dividing the highest analyte ion signal intensity from the entire data set by the highest analyte ion signal intensity from the data obtained for no counter flow. A and B denote [Val⁵]-angiotensin I and bradykinin, respectively.

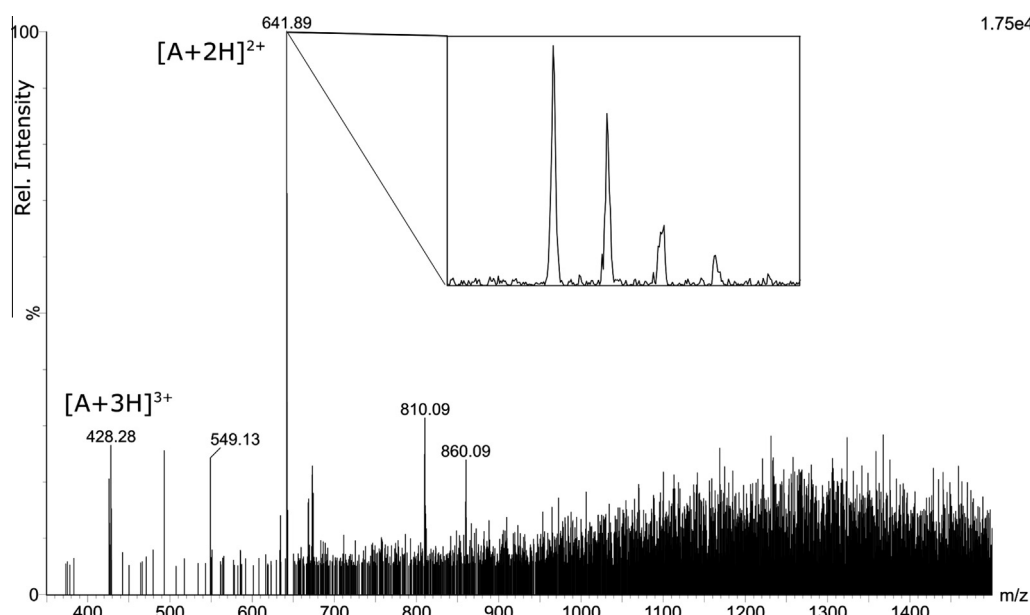**Fig. 7.** Liquid AP-MALDI mass spectrum of 1 fmol of [Val⁵]-angiotensin I. A total of 300 scans (1 s per scan) were combined. Singly charged ion signals were filtered out. Inset shows the zoomed-in region of the doubly protonated [Val⁵]-angiotensin I species.

above observations (Fig. 3b). Interestingly, the intensity of the triply protonated [Val⁵]-angiotensin I species slightly increases with increasing distance contrary to the anticipated decrease due to less efficient sampling (or lower ion extraction field). Such behaviour can be explained by the increased travel distance and transit time facilitating the droplets desolvation.

3.2. Generation of multiply protonated analytes with heating of the ion transfer tube

Heated ion transfer tubes (capillaries) are often used to promote desolvation of the desorbed clusters and droplets, thus supporting the efficient generation of molecular analyte ions [44,57]. The desolvation efficiency in such ion transfer tubes depends on the temperature and cluster/droplet residence time in the heated region.

Both temperature and cluster/droplet residence time are affected by the gas flow rate. High flow rates provide more efficient cooling of the tube's wall temperature. Moreover, due to insufficient time for reaching thermal equilibrium the gas temperature inside the ion transfer tube may be sufficiently cooler than the tube's wall temperature, depending on the geometry of the tube and heated area and the flow speed. The cluster/droplet residence time inside the ion transfer tube also depends on the gas flow velocity, and on the initial ion or droplet velocity, which is affected by the geometry and electrical fields of the ion source. Therefore, to build an efficient desolvation device the above parameters need to be carefully considered. The gas flow values are predicated by the geometry of the ion transfer tube, *i.e.* by its inner diameter, the size of the inlet and exit apertures, and its length. By varying these parameters the residence time and the gas temperature distribution inside the ion

transfer tube may be adjusted. However, such adjustments require hardware modification and are therefore difficult to optimize and unsuitable for *ad hoc* tuning. The other possibility to adjust the gas flow velocity is to control the pressure at the ion transfer tube's exit, *e.g.* by introducing a counter gas flow. The latter can be achieved by infusing gas between the exit of the heated region/ion transfer tube and the inlet to the mass spectrometer as shown in Fig. 1. Such a set-up allows the partial optimization of the desolvation conditions and was applied in the following experiments.

The counter gas flow used was variable and at higher values able to reverse the direction of the flow inside the ion transfer tube, preventing any ions from the ion source to reach the mass analyzer. At a software-set value of 265 L/h for the counter gas infusion, ion signals disappeared in experiments where ions were generated by thermal ionization in the overheated ion transfer tube, which generally provided a very stable ion signal under normal conditions (*i.e.* counter gas flow sufficiently below this threshold value). Thus, it can be assumed that at this value the counter gas flow resulted in zero gas flow in the ion transfer tube. In addition, analyte ion signals simultaneously measured in these experiments also disappeared at this threshold flow. Therefore, this value can be taken as a reasonable upper limit for good ion transmission without incurring losses due to reversed gas flow.

As the ion transfer tube wall temperature and the temperature inside the ion transfer tube depend on the gas flow, the effect of gas flow on the gas and tube temperature was measured and correlated against the observed analyte ion signal. For this investigation the heating power applied to the NiCr wire was varied between 0 W and 60 W in steps of 10 W, and the counter flow was varied in the range of 0–252 L/h in steps of 42 L/h. Each measurement series was started with the largest counter flow value of 252 L/h and the ion transfer tube was conditioned for 2 min before the data were acquired, ensuring that the temperature reached equilibrium. The counter flow gas value was then sequentially dropped and the ion transfer tube was left for at least 1 min before each single temperature measurement was undertaken. A total of 20 data points with a sampling rate of 1 acquisition per second were averaged for each gas flow-heating power setting.

While the measurements of the ion transfer tube wall temperature arguably provided fairly accurate values, the measurements of the temperature inside the ion transfer tube were less accurate owing to the influence of the thermocouple on the gas flow and the difficulty in determining its exact location in the ion transfer tube. However, as the position of the thermocouple inside the ion transfer tube was not changed throughout an experiment, the measured temperature values can at least provide a trend of the temperature dependency on the applied heat and gas flow.

In Fig. 4, the measured values of the wall temperature and temperature inside the ion transfer tube are shown for the various heating power and counter flow settings. The right columns in both plots represent the flow conditions close to zero (stationary) flow. From the data it can be seen that both the wall temperature and the inner temperature significantly and monotonically decrease with a decrease in the heating power. Both temperatures also similarly decrease with an increase in counter flow, *i.e.* a decrease in gas flow in the ion transfer tube, though with a slower relative rate for the outside wall temperature and the exception of the temperatures at 0 W heating power.

Using the above set-up the analyte ion charge state was then studied with respect to its dependency on the desolvation conditions. A liquid MALDI sample with 5 pmol of each [Val[5]]-angiotensin I and bradykinin was loaded on the target. The laser energy was attenuated to 16 µJ and the laser beam was focused to a diameter of approximately 100–150 µm. The target plate potential was set to 3 kV and the distance between the ion transfer tube and target plate was 3 mm.

In Fig. 5, intensity maps are shown for singly, doubly and triply protonated [Val[5]]-angiotensin I species. For all analyte ion species the greatest signal intensities are not found at the highest heating power or the highest counter flow, *i.e.* lowest gas flow in the transfer tube towards the mass analyzer. Also, the highest signal intensities for singly protonated analytes can be found at higher counter flows and higher heating power compared to the doubly and triply protonated analytes. Ignoring the data obtained from the conditions close to zero flow (*i.e.* counter flow of 252 L/h), it can be seen that for the singly protonated species the difference in signal intensity is around two orders of magnitude between the lowest and highest values while for the triply protonated molecules this difference is an order of magnitude greater.

Importantly, from these three-dimensional plots it can be easily seen that there is a clear difference in optimal temperature and residence time in the ion transfer region for the detection of singly protonated analytes compared to doubly and triply protonated species. According to this data, higher charge state ions require a cooler environment for efficient molecular ion generation and transmission. A similar behaviour was observed in ESI, and a model explaining such behaviour was proposed [52,53]. Arguably, this difference can be explained by the higher mobility of multiply protonated species once liberated from the cluster/droplet, accelerating these ion species due to their greater charge much faster to the ion transfer tube wall where they will be lost. Thus, residence times in the ion transfer tube need to be shorter for multiply protonated molecules compared to singly protonated molecules if the same relative ion transmission is to be achieved. The lower abundance of higher protonated molecules at higher temperatures might also be explained through proton loss and more efficient fragmentation of the higher protonated species owing to additional Coulomb repulsion as a result of thermal activation via CID with the entrainment gas or through surface-induced dissociation (SID) at the wall of the ion transfer tube [58,59].

In agreement with other studies [19,20], the ion signal intensities for all counter gas flow values at 0 W heating power are higher for singly than for multiply protonated angiotensin molecules (apart from the intensity at the counter gas flow of 252 L/h – *vide supra*). This in combination with the much slower increase in ion signal intensity of the singly protonated species with heating power is also in agreement with the previously reported relative signal intensity change to predominantly multiply charged species with an increase in temperature of the ion transfer region [20]. This behaviour was particularly well observed at counter gas flow rates between ~100 and 200 L/h, which led to gas flow velocities that probably reflect best the gas flow velocity of a previously used ion source geometry by Cramer *et al.* [20] where the inner diameter of the ion transfer tube is twice as large as the one in these experiments. Supplemental Fig. 1 shows this change for the counter gas flows of 126, 168 and 210 L/h using the spectra obtained at a heating power of 0 W and 20 W, which results in a similar wall temperature of the ion transfer tube (~200–300 °C) as employed by Cramer *et al.* [20].

However, in general it was found that larger inner diameters of the ion transfer tube resulted in slightly lower absolute analyte ion yields and were therefore not further pursued. It is worth noting that other changes of the ion source geometry also led to significant shifts in the relative ion signal intensities as can be seen by the example of changing the restriction cone orifice (*cf.* Fig. 1) from 0.8 mm to 0.5 mm or 0.67 mm (see Supplemental Figs. 2 and 3).

Overall, these data reveal the importance of other parameters than just the temperature in the ion transfer region for achieving optimal detection of multiply protonated analytes in liquid MALDI MS. Although the ion yield of singly protonated species can also be further optimized by adjusting the (counter) gas flow, it is clear that the greater effect of gas flow optimization can be seen for

the ion yield of multiply protonated species. Fig. 6 demonstrates the differences in ion signal enhancement for the various ion species when both heating power and gas flow are optimized compared to heating power alone. For this figure, the same raw data used for Fig. 5 was further analyzed by dividing the highest ion signal intensity from the entire data set by the highest ion signal intensity from the data obtained for no counter flow (*cf.* first column of the heat maps in Fig. 5), which represent the data points for the situation of optimizing the ion yield by adjusting only the ion transfer tube wall temperature. As can be seen in Fig. 6 the highest gain is obtained for the multiply protonated species.

The above data further supports the hypothesis that the formation of singly protonated species is distinctly different to the generation of multiply protonated molecules. The latter may be generated solely through an ESI-like droplet desolvation/evaporation process predominantly in the heated ion transfer region. Thus, a more uniform heat distribution as well as less turbulent flow regime may help to promote a more spatially (optimally) confined release of the analyte ions in the tube, and therefore, these ions could become less prone to the losses on the wall of the ion transfer tube.

For optimum sensitivity it has also been found that lowering the amount of DHB in the liquid MALDI sample as well as operating the laser just above the ionization threshold increases the signal-to-noise level (data not shown). Fig. 7 shows a representative spectrum of 1 fmol of [Val^5]-angiotensin I acquired at heating power and counter gas flow values optimal for the sensitive detection of multiply protonated analytes. For this acquisition the liquid matrix was prepared with 25 mg/mL DHB and 60% glycerol addition as described earlier. The laser energy was attenuated to 8.35 µJ and the laser spot size was ∼100–150 µm. The gap between the ion transfer tube and the target plate was 3 mm and the applied potential was 4 kV. The data was acquired with drift time recording enabled and the singly charged ion signals were filtered out from the spectrum.

Further information about the data supporting these results and requests for access to the data can be directed to the corresponding author.

4. Conclusions

This study shows that MS ion source parameters play a significant role for the efficient generation and detection of multiply protonated analytes in liquid AP-MALDI MS. The differences in response to parameter changes between singly and multiply protonated analytes support the hypothesis that singly protonated molecules are predominantly produced by classical MALDI processes earlier in time and closer to the sample surface while multiply protonated molecules are rather produced by ESI-like processes, and therefore more dependent on parameter changes further in the ionization interface/ion transfer region. However, the acquired data also show that the desolvation conditions are significantly different to those typically applied to nano-ESI plumes. As such an additional heated region provides a significant improvement in the ion source performance for the generation of multiply protonated analytes by liquid MALDI MS. Our initial optimization studies show that for the ion source geometries tested it was beneficial to control the flow regime in the heated ion transfer region. Optimization of the applied heat and flow conditions inside the heated ion transfer region resulted in an ion yield gain of up to 14 times based on the detected signal intensity for multiply protonated peptides.

Acknowledgements

Appendix A. Supplementary data

Supplementary data associated with this article can be found, in the online version, at http://dx.doi.org/10.1016/j.ymeth.2016.01.015.

References

[1] M. Karas, D. Bachmann, F. Hillenkamp, Matrix-assisted ultraviolet laser desorption of non-volatile compounds, Int. J. Mass Spectrom. Ion Processes 78 (1987) 53–68.

[2] M. Karas, F. Hillenkamp, Laser desorption ionization of proteins with molecular masses exceeding 10,000 daltons, Anal. Chem. 60 (1988) 2299–2301.

[3] J.B. Fenn, M. Mann, C.K. Meng, S.F. Wong, C.M. Whitehouse, Electrospray ionization for mass spectrometry of large biomolecules, Science 246 (1989) 64–71.

[4] J.G. Boyle, C.M. Whitehouse, Time-of-flight mass spectrometry with an electrospray ion beam, Anal. Chem. 64 (1992) 2084–2089.

[5] A.F. Dodonov, I.V. Chernushevich, V.V. Laiko, Electrospray ionization on a reflecting time-of-flight mass spectrometer, in: R.J. Cotter (Ed.), Time-of-Flight Mass Spectrometry, American Chemical Society, 1994, pp. 108–123.

[6] G.L. Glish, D.J. Burinsky, Hybrid mass spectrometers for tandem mass spectrometry, J. Am. Soc. Mass Spectrom. 19 (2011) 161–172.

[7] A.B. Kanu, P. Dwivedi, M. Tam, L. Matz, H.H. Hill, Ion mobility–mass spectrometry, J. Mass Spectrom. 43 (2008) 1–22.

[8] E. Mirgorodskaya, C. Braeuer, P. Fucini, H. Lehrach, J. Gobom, Nanoflow liquid chromatography coupled to matrix-assisted laser desorption/ionization mass spectrometry: sample preparation, data analysis, and application to the analysis of complex peptide mixtures, Proteomics 5 (2005) 399–408.

[9] A. Zerck, E. Nordhoff, H. Lehrach, K. Reinert, Optimal precursor ion selection for LC–MALDI MS/MS, BMC Bioinform. 14 (2013) 1–14.

[10] K. Wiangnon, R. Cramer, Liquid MALDI MS analysis of complex peptide and proteome samples (in preparation).

[11] J. Qin, B.T. Chait, Matrix-assisted laser desorption ion trap mass spectrometry: efficient isolation and effective fragmentation of peptide ions, Anal. Chem. 68 (1996) 2108–2112.

[12] A.V. Loboda, A.N. Krutchinsky, M. Bromirski, W. Ens, K.G. Standing, A tandem quadrupole/time-of-flight mass spectrometer with a matrix-assisted laser desorption/ionization source: design and performance, Rapid Commun. Mass Spectrom. 14 (2000) 1047–1057.

[13] K.F. Medzihradszky, J.M. Campbell, M.A. Baldwin, A.M. Falick, P. Juhasz, M.L. Vestal, A.L. Burlingame, The characteristics of peptide collision-induced dissociation using a high-performance MALDI-TOF/TOF tandem mass spectrometer, Anal. Chem. 72 (2000) 552–558.

[14] K.J. Gillig, B. Ruotolo, E.G. Stone, D.H. Russell, K. Fuhrer, M. Gonin, A.J. Schultz, Coupling high-pressure MALDI with ion mobility/orthogonal time-of-flight mass spectrometry, Anal. Chem. 72 (2000) 3965–3971.

[15] V.V. Laiko, M.A. Baldwin, A.L. Burlingame, Atmospheric pressure matrix-assisted laser desorption/ionization mass spectrometry, Anal. Chem. 72 (2000) 652–657.

[16] K.A. Kellersberger, P.V. Tan, V.V. Laiko, V.M. Doroshenko, D. Fabris, Atmospheric pressure MALDI-Fourier transform mass spectrometry, Anal. Chem. 76 (2004) 3930–3934.

[17] J.-L. Wolfender, F. Chu, H. Ball, F. Wolfender, M. Fainzilber, M.A. Baldwin, A.L. Burlingame, Identification of tyrosine sulfation in *Conus pennaceus* conotoxins α-PnIA and α-PnIB: further investigation of labile sulfo- and phosphopeptides by electrospray, matrix-assisted laser desorption/ionization (MALDI) and atmospheric pressure MALDI mass spectrometry, J. Mass Spectrom. 34 (1999) 447–454.

[18] S. König, O. Kollas, K. Dreisewerd, Generation of highly charged peptide and protein ions by atmospheric pressure matrix-assisted infrared laser desorption/ionization ion trap mass spectrometry, Anal. Chem. 79 (2007) 5484–5488.

[19] S. Trimpin, E.D. Inutan, T.N. Herath, C.N. McEwen, Laserspray ionization, a new atmospheric pressure MALDI method for producing highly charged gas-phase ions of peptides and proteins directly from solid solutions, Mol. Cell Proteomics 9 (2010) 362–367.

[20] R. Cramer, A. Pirkl, F. Hillenkamp, K. Dreisewerd, Liquid AP-UV-MALDI enables stable ion yields of multiply charged peptide and protein ions for sensitive analysis by mass spectrometry, Angew. Chem. Int. Ed. Engl. 52 (2013) 2364–2367.

[21] G. Westmacott, M. Frank, S.E. Labov, W.H. Benner, Using a superconducting tunnel junction detector to measure the secondary electron emission efficiency for a microchannel plate detector bombarded by large molecular ions, Rapid Commun. Mass Spectrom. 14 (2000) 1854–1861.

[22] A. Makarov, Electrostatic axially harmonic orbital trapping: a high-performance technique of mass analysis, Anal. Chem. 72 (2000) 1156–1162.

[23] A.G. Marshall, C.L. Hendrickson, G.S. Jackson, Fourier transform ion cyclotron resonance mass spectrometry: a primer, Mass Spectrom. Rev. 17 (1998) 1–35.
[24] D.J. Douglas, Linear quadrupoles in mass spectrometry, Mass Spectrom. Rev. 28 (2009) 937–960.
[25] R. Cramer, S. Corless, The nature of collision-induced dissociation processes of doubly protonated peptides: comparative study for the future use of matrix-assisted laser desorption/ionization on a hybrid quadrupole time-of-flight mass spectrometer in proteomics, Rapid Commun. Mass Spectrom. 15 (2001) 2058–2066.
[26] D.M. Good, M. Wirtala, G.C. McAlister, J.J. Coon, Performance characteristics of electron transfer dissociation mass spectrometry, Mol. Cell Proteomics 6 (2007) 1942–1951.
[27] Y. Huang, J.M. Triscari, G.C. Tseng, L. Pasa-Tolic, M.S. Lipton, R.D. Smith, V.H. Wysocki, Statistical characterization of the charge state and residue dependence of low-energy CID peptide dissociation patterns, Anal. Chem. 77 (2005) 5800–5813.
[28] R.A. Zubarev, N.L. Kelleher, F.W. McLafferty, Electron capture dissociation of multiply charged protein cations. A nonergodic process, J. Am. Chem. Soc. 120 (1998) 3265–3266.
[29] J.E.P. Syka, J.J. Coon, M.J. Schroeder, J. Shabanowitz, D.F. Hunt, Peptide and protein sequence analysis by electron transfer dissociation mass spectrometry, Proc. Nat. Acad. Sci. U.S.A. 101 (2004) 9528–9533.
[30] H. Ehring, M. Karas, F. Hillenkamp, Role of photoionization and photochemistry in ionization processes of organic molecules and relevance for matrix-assisted laser desorption Ionization mass spectrometry, Org. Mass Spectrom. 27 (1992) 472–480.
[31] R. Zenobi, R. Knochenmuss, Ion formation in MALDI mass spectrometry, Mass Spectrom. Rev. 17 (1998) 337–366.
[32] R. Knochenmuss, R. Zenobi, MALDI ionization: the role of in-plume processes, Chem. Rev. 103 (2003) 441–452.
[33] R. Knochenmuss, Ion formation mechanisms in UV-MALDI, Analyst 131 (2006) 966–986.
[34] M. Karas, M. Glückmann, J. Schäfer, Ionization in matrix-assisted laser desorption/ionization: singly charged molecular ions are the lucky survivors, J. Mass Spectrom. 35 (2000) 1–12.
[35] M. Karas, R. Krüger, Ion formation in MALDI: the cluster ionization mechanism, Chem. Rev. 103 (2003) 427–440.
[36] R. Knochenmuss, L.V. Zhigilei, What determines MALDI ion yields? A molecular dynamics study of ion loss mechanisms, Anal. Bioanal. Chem. 402 (2011) 2511–2519.
[37] V. Frankevich, J. Zhang, M. Dashtiev, R. Zenobi, Production and fragmentation of multiply charged ions in 'electron-free' matrix-assisted laser desorption/ionization, Rapid Commun. Mass Spectrom. 17 (2003) 2343–2348.
[38] M. Dole, L.L. Mack, R.L. Hines, R.C. Mobley, L.D. Ferguson, M.B. Alice, Molecular beams of macroions, J. Chem. Phys. 49 (1968) 2240–2249.
[39] J.V. Iribarne, B.A. Thomson, On the evaporation of small ions from charged droplets, J. Chem. Phys. 64 (1976) 2287–2294.
[40] B.A. Thomson, J.V. Iribarne, Field induced ion evaporation from liquid surfaces at atmospheric pressure, J. Chem. Phys. 71 (1979) 4451–4463.
[41] P. Kebarle, U.H. Verkerk, On the mechanism of electrospray ionization mass spectrometry (ESIMS), in: R.B. Cole (Ed.), Electrospray and MALDI Mass Spectrometry: Fundamentals, Instrumentation, Practicalities, and Biological Applications, second ed., John Wiley & Sons Inc., 2010, pp. 1–48.
[42] M. Yamashita, J.B. Fenn, Negative ion production with the electrospray ion source, J. Phys. Chem. 88 (1984) 4671–4675.
[43] C.M. Whitehouse, R.N. Dreyer, M. Yamashita, J.B. Fenn, Electrospray interface for liquid chromatographs and mass spectrometers, Anal. Chem. 57 (1985) 675–679.
[44] S.K. Chowdhury, V. Katta, B.T. Chait, An electrospray-ionization mass spectrometer with new features, Rapid Commun. Mass Spectrom. 4 (1990) 81–87.
[45] A.T. Navare, F.M. Fernández, Inline pneumatically assisted atmospheric pressure matrix-assisted laser desorption/ionization ion trap mass spectrometry, J. Mass Spectrom. 45 (2010) 635–642.
[46] B.B. Schneider, C. Lock, T.R. Covey, AP and vacuum MALDI on a QqLIT instrument, J. Am. Soc. Mass Spectrom. 16 (2005) 176–182.
[47] C.A. Miller, D. Yi, P.D. Perkins, An atmospheric pressure matrix-assisted laser desorption/ionization ion trap with enhanced sensitivity, Rapid Commun. Mass Spectrom. 17 (2003) 860–868.
[48] M. Pauly, M. Sroka, J. Reiss, G. Rinke, A. Albarghash, R. Vogelgesang, H. Hahne, B. Kuster, J. Sesterhenn, K. Kern, S. Rauschenbach, A hydrodynamically optimized nano-electrospray ionization source and vacuum interface, Analyst 139 (2014) 1856–1867.
[49] L. Zhou, B. Yue, D.V. Dearden, E.D. Lee, A.L. Rockwood, M.L. Lee, Incorporation of a venturi device in electrospray ionization, Anal. Chem. 75 (2003) 5978–5983.
[50] R. Ramanathan, N. Raghavan, S.N. Comezoglu, W.G. Humphreys, A low flow ionization technique to integrate quantitative and qualitative small molecule bioanalysis, Int. J. Mass Spectrom. 301 (2011) 127–135.
[51] Z. Takáts, J.M. Wiseman, B. Gologan, R.G. Cooks, Electrosonic spray ionization. A gentle technique for generating folded proteins and protein complexes in the gas phase and for studying ion–molecule reactions at atmospheric pressure, Anal. Chem. 76 (2004) 4050–4058.
[52] J.S. Page, R.T. Kelly, K. Tang, R.D. Smith, Ionization and transmission efficiency in an electrospray ionization-mass spectrometry interface, J. Am. Soc. Mass Spectrom. 18 (2007) 1582–1590.
[53] J.S. Page, I. Marginean, E.S. Baker, R.T. Kelly, K. Tang, R.D. Smith, Biases in ion transmission through an electrospray ionization-mass spectrometry capillary inlet, J. Am. Soc. Mass Spectrom. 20 (2009) 2265–2272.
[54] D. Kessner, M. Chambers, R. Burke, D. Agus, P. Mallick, ProteoWizard: open source software for rapid proteomics tools development, Bioinformatics 24 (2008) 2534–2536.
[55] BatMass. 2015/10/13/10:39:33; Available from: <http://www.batmass.org/>.
[56] C.N. McEwen, B.S. Larsen, S. Trimpin, Laserspray ionization on a commercial atmospheric pressure-MALDI mass spectrometer ion source: selecting singly or multiply charged ions, Anal. Chem. 82 (2010) 4998–5001.
[57] T. Kim, H.R. Udseth, R.D. Smith, Improved ion transmission from atmospheric pressure to high vacuum using a multicapillary inlet and electrodynamic ion funnel interface, Anal. Chem. 72 (2000) 5014–5019.
[58] R.B. Cole, Some tenets pertaining to electrospray ionization mass spectrometry, J. Mass Spectrom. 35 (2000) 763–772.
[59] Y. Li, R.B. Cole, Charge state distributions in electrospray and MALDI, in: R.B. Cole (Ed.), Electrospray and MALDI Mass Spectrometry: Fundamentals, Instrumentation, Practicalities, and Biological Applications, second ed., John Wiley & Sons Inc., 2010, pp. 491–534.